

# Pushing the Limits of Heat Conduction in Covalent Organic Frameworks Through High-Throughput Screening of Their Thermal Conductivity

Sandip Thakur and Ashutosh Giri\*

Tailor-made materials featuring large tunability in their thermal transport properties are highly sought-after for diverse applications. However, achieving 'user-defined' thermal transport in a single class of material system with tunability across a wide range of thermal conductivity values requires a thorough understanding of the structure-property relationships, which has proven to be challenging. Herein, large-scale computational screening of covalent organic frameworks (COFs) for thermal conductivity is performed, providing a comprehensive understanding of their structure-property relationships by leveraging systematic atomistic simulations of 10,750 COFs with 651 distinct organic linkers. Through the data-driven approach, it is shown that by strategic modulation of their chemical and structural features, the thermal conductivity can be tuned from ultralow ( $\approx 0.02 \text{ W m}^{-1} \text{ K}^{-1}$ ) to exceptionally high (≈50 W m<sup>-1</sup> K<sup>-1</sup>) values. It is revealed that achieving high thermal conductivity in COFs requires their assembly through carbon-carbon linkages with densities greater than 500 kg m<sup>-3</sup>, nominal void fractions (in the range of  $\approx$ 0.6–0.9) and highly aligned polymeric chains along the heat flow direction. Following these criteria, it is shown that these flexible polymeric materials can possess exceptionally high thermal conductivities, on par with several fully dense inorganic materials. As such, the work reveals that COFs mark a new regime of materials design that combines high thermal conductivities with low densities.

### 1. Introduction

With a diverse choice of molecular building blocks and linkage chemistries, covalent organic frameworks (COFs) represent

S. Thakur, A. Giri Department of Mechanical Industrial, and Systems Engineering University of Rhode Island Kingston, RI 02881, USA E-mail: ashgiri@uri.edu

The ORCID identification number(s) for the author(s) of this article can be found under https://doi.org/10.1002/smll.202401702

© 2024 The Authors. Small published by Wiley-VCH GmbH. This is an open access article under the terms of the Creative Commons Attribution-NonCommercial-NoDerivs License, which permits use and distribution in any medium, provided the original work is properly cited, the use is non-commercial and no modifications or adaptations are made.

DOI: 10.1002/smll.202401702

an emerging class of porous crystalline materials with highly modular architectures and an unbounded potential for tailormade design in various applications.[1-7] For instance, their high internal surface areas and large void fractions combined with their enhanced thermal stabilities, as compared to their metal organic framework (MOF)-cousins,[8] make them ideal candidates for gas storage and separation,[4,5,9-13] catalysis,[14-17] chemical sensing,[18,19] biomedical applications,[20] drug delivery,[20,21] thermoelectrics, thermal barrier coatings,[22-27] and the next generation of energy storage materials.[12,28-31] Central to these applications, is their ability to dissipate heat (as quantified by their thermal conductivity,  $\kappa$ ). This is most notably exemplified in gas storage applications, where the exothermic processes of adsorption of guest species can raise the internal temperatures of the nanoporous open frameworks up to several hundereds of Kelvin (especially during high loading rates of adsorbed gases).[32,33] For such applications, it is highly desirable for COFs to possess high thermal conductivities for efficient heat dissipation. On the other

hand, for applications in thermal barrier coatings and thermoelectrics, it is required that the materials demonstrate low lattice thermal conductivities, [34-37] which is ideally suited for framework materials with high porosities. [26,38,39]

The immense design space for the internal architecture of COFs (based on various chemical linkages and morphologies) presents a unique platform to not only engineer ultralow thermal conductivities in these porous materials, but also attain high thermal conductivities. This is typically not achievable in other porous crystals such as MOFs and zeolites, which have been mostly associated with glass-like thermal conductivities in the range of  $\approx\!0.3$  to 1 W m $^{-1}$  K $^{-1}$ .[23,24,32,33,38,40–57] In this regard, the better heat conduction in COFs was first shown in the recent work by Evans et al.,[58] where they measured relatively high thermal conductivities of  $\approx\!1$  W m $^{-1}$  K $^{-1}$  across the non-bonded direction of boronate ester-linked 2D COFs. Furthermore, they also demonstrated that the thermal conductivities along the bonded (in-plane) directions are about four times higher in comparison to the (cross-plane) direction with the van der Waals interactions,



conduction through additional vibrational scattering.[38,66] With the exception of the experimental results from Evans et al., [58] insights into the thermal transport processes in COFs have mostly relied on molecular dynamics (MD) simulations. [25,26,59-62,64,65,67-70] Although these simulations are inherently limited by the accuracy of the force fields utilized, they nonetheless provide critical insights into qualitative trends and intrinsic vibrational scattering mechanisms dictating heat conduction in porous crystals. For instance, Giri and Hopkins have shown that gas infiltration can be used as an efficient 'knob' to tune the thermal conductivity of 2D COFs with laminar pore channels.[61] Moreover, Rahman et al. have elucidated that filling the pores of 2D COFs with methane can either increase or decrease the overall thermal conductivity, depending on the characteristic sizes of the laminar pore channels.[25] Similarly, the pore geometry and overall density have been shown to drive thermal transport for both 2D and 3D COFs, where higher densities are generally associated with COFs possessing relatively higher thermal conductivities.<sup>[26,64,65]</sup> In fact, interpenetration of COF-300, which results in an increase in the density of the structure, has also been shown to drastically increase their thermal conductivites (by as much as sixfold for a threefold interpenetration of the COF-300 open framework) through supramolecular interactions, [59] thus providing another useful strategy with which to control the intrinsic vibrational scattering mechanisms in COFs.

thus paving the way for engineering high thermal conductivities

along the strongly bonded and highly modular polymeric chains.

Following Evans et al.'s work, several studies have also unveiled that COFs can exhibit higher thermal conductivities compared to

MOFs and zeolites.<sup>[25-27,58-65]</sup> This has mainly been attributed to

the extended crystalline frameworks in COFs that are composed

of strongly bonded light atoms (e.g., C, N, O, and B). In contrast,

the large atomic mass mismatches associated with the nodes con-

taining the heavy metal atoms and the linkers composed of light-

mass organic molecules in MOFs can significantly impede heat

Although the above mentioned studies have laid the groundwork toward a more comprehensive understanding of the intrinsic mechanisms dictating thermal transport in COFs, these studies have only focused on a very small subset of COFs, making it difficult to extend the conclusions for wider ranges of COFs. For example, COFs (and porous crystals in general), are known for their large chemical and structural tunabilities, giving rise to an overwhelmingly large "COF-space" that cannot be comprehensively explored without a systematic data-driven approach. Such an approach that explores large numbers of linker chemistries and diverse topologies of COFs is needed to provide conclusive structure-property relationships, which is the central goal of this work.

To this end, we employ high-throughput MD simulations to calculate thermal conductivities of 10,750 diverse 3D COFs with 651 distinct organic linkers and four types of covalent linkages. [71] This data-driven approach allows us to not only unveil critical insights into their structure-property relationships, but also identify several COFs with ultralow and exceptionally high thermal conductivities. Specifically, to achieve high thermal conductivity in these porous crystals, we show that their structure should be made up of carbon-carbon linkages with polymeric chains that are well-aligned to the direction of heat flow, possess densities in the range of 500 to 900 kg  $m^{-3}$  with pore sizes <15 Å, void fractions between 0.6 to 0.9 and geometric surface areas (GSA) in the range of 2,000 to 4,000  $m^2$   $g^{-1}$ . Through this intricate balance of structural and chemical parameters, we identify 14 COFs with thermal conductivities > 10 W m<sup>-1</sup> K<sup>-1</sup> that includes COFs with thermal conductivities that can reach as high as 47 W m<sup>-1</sup> K<sup>-1</sup>, on par with several fully dense semiconductors such as GaAs.<sup>[72]</sup> Likewise, we identify 94 COFs with ultralow thermal conductivities ( $\leq 0.05 \text{ W m}^{-1} \text{ K}^{-1}$ ), low densities ( $\leq 150 \text{ kg m}^{-3}$ ), and large pore sizes (>45 Å). To achieve low thermal conductivities (<0.2 W m<sup>-1</sup> K<sup>-1</sup>) at relatively higher densities, we show that the linkers should contain heavier atoms such as silicon and sulfur that can present additional scattering channels through mass and bond disorders. Finally, we also show that COFs with thermal conductivities in the range of 0.2 to 1 W  $m^{-1}$  K $^{-1}$  are associated with high methane uptakes (>180  $v_{STP}/v$ ). We also reveal the combination of optimized structural parameters that leads to high deliverable capacities and high thermal conductivities, thus providing critical insights into the design of COFs with high gas storage capacities along with efficient heat dissipation capabilities.

## 2. Results and Discussion

The 10,750 3D COFs are taken from the database as reported by Mercado et al.<sup>[71]</sup> We choose COFs that span 234 unique topologies with 651 distinct linkers for our high-throughput calculations of thermal conductivity. Representative linker building blocks for several COFs that demonstrate exceptionally low and high thermal conductivities (as discussed in more detail below) are shown in **Figure 1**. It is important to note that the four types of covalent linkages (namely, carbon-carbon, imine, amine, and amide bonds) were chosen to ensure reversible bond formation on a time scale allowing for corrections to defect formations during the self-assembly process and thus facilitating the formation of extended crystalline structures with strong covalent bonds.[5,71,73]

Figure 2a summarizes our calculations of the average thermal conductivity,  $\kappa_{avg}$ , (which is the average of values along x-, y-, and z-directions) for all of the 10,750 COFs studied. Not surprisingly, and in agreement with previous studies that have shown a linear relationship between  $\kappa$  and COF density, [26,39] the thermal conductivity, in general, increases with density of the COFs. However, for one particular density, the thermal conductivities can have a broad range of values. For instance, at  $700 \text{ kg m}^{-3}$ , thermal conductivities span from 0.3 W m<sup>-1</sup> K<sup>-1</sup> to approximately 10 W m<sup>-1</sup> K<sup>-1</sup>. Therefore, while density correlates with thermal conductivity, density alone is insufficient to account for the observed variations in thermal conductivity. We note that as density (or the structure porosity) is an important metric for the design of COFs for several targeted applications such as gas storage, in what follows, we will discuss how this property correlates with other geometrical factors such as GSA, largest pore diameter (LPD) and void fractions to determine the thermal conductivity of COFs. From our analysis below, we will be able to identify unique structure-property relationships such as the combinations of relatively low density and high thermal conductivity or low thermal conductivity with relatively high density in COFs, which is difficult to realize without high-throughput screening of a large and diverse COF dataset as carried out here.

linker94

www.advancedsciencenews.com

linker111

www.small-journal.com

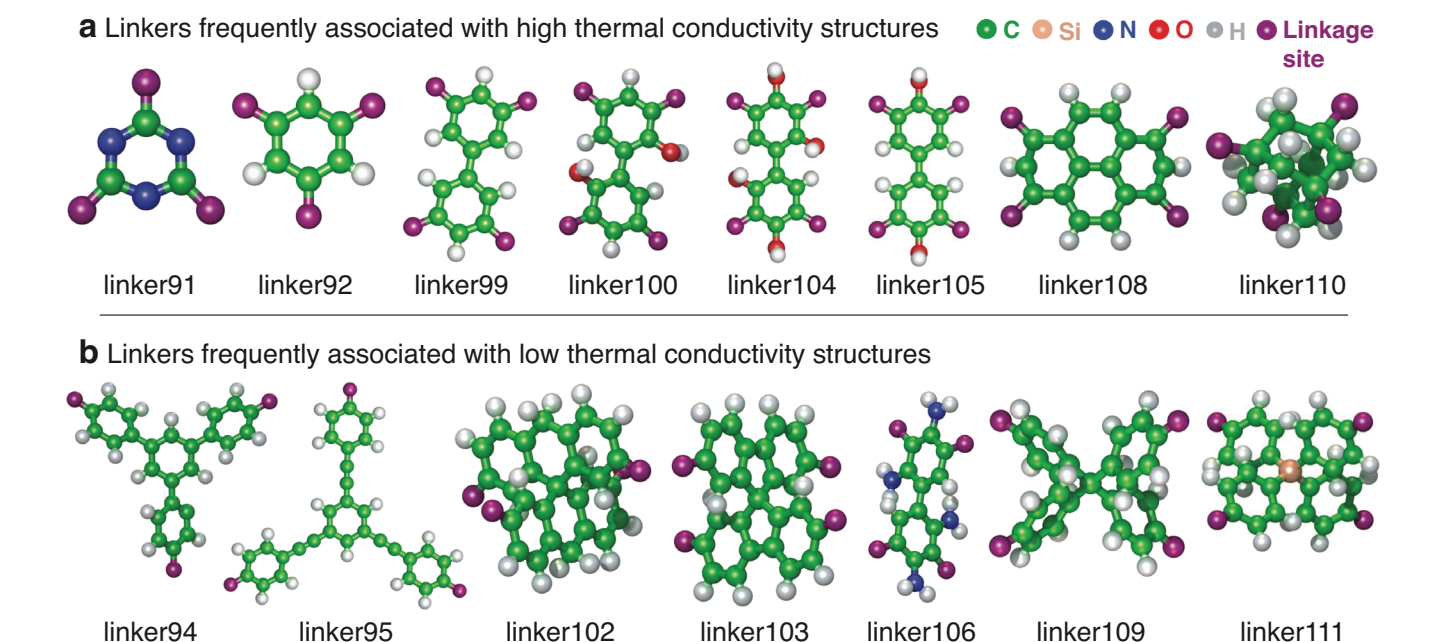


Figure 1. Schematic illustration of several characteristic linkers that are most frequently associated with (a) high and (b) low thermal conductivities in 3D COFs

linker102

Considering the various linker chemistry selections, it is evident from Figure 2a that COFs with carbon-carbon linkages not only possess relatively higher densities, but also exhibit higher thermal conductivities. In fact, almost all COFs that have  $\kappa > 1$ W m<sup>-1</sup> K<sup>-1</sup> are made up of carbon–carbon linkages. This is likely due to the fact that the COFs formed with the shorter carboncarbon bonds result in frameworks with relatively higher densities and ones with stronger covalent bonds that better facilitate heat conduction as compared to their amide, amine, and imine bonded counterparts. As such, a key consideration for designing COFs with high thermal conductivities is the selection of carbon-carbon linkages for the bond-formation chemistry. While our study primarily focuses on the influence of bond linkages, it is worth noting that functional groups could also significantly influence the vibrational properties of COFs. However, quantitatively determining the contributions of various functional groups to thermal transport would require a detailed analysis and a separate effort, which is beyond the scope of the current work.

Overall, from the 10,750 3D COFs, about 97% possess  $\kappa_{avg}$  $\leq$ 1 W m<sup>-1</sup> K<sup>-1</sup> as shown in Figure 2b. We only find 15 COFs with  $\kappa_{\rm avg} \geqslant 5~{\rm W~m^{-1}~K^{-1}}$  and among these COFs, three possess  $\kappa_{\rm avg} > 10~{\rm W~m^{-1}~K^{-1}}$ . In this regard, the highest predicted  $\kappa_{\rm avg}$  is approximately 20 W m<sup>-1</sup> K<sup>-1</sup> for a carbon–carbon linked COF with a density of 980 kg m<sup>-3</sup> (the schematic of which is shown in Figure 2c). However, this particular COF structure is highly anisotropic with a thermal conductivity anisotropy ratio of  $\approx 9$ demonstrating ultra-high thermal conductivity in one direction and relatively lower thermal conductivities in the other two directions (9.8, 5.5, and 47 W m<sup>-1</sup> K<sup>-1</sup> in x-, y-, and z-directions, respectively). In fact, about 35% of the COFs studied exhibit anisotropic thermal conductivities, with anisotropy ratios exceeding 1.5 (that is higher than 50% thermal conductivity in one principal direction as compared to the minimum thermal conductivity of the

other two principal directions). It is also noteworthy that the maximum anisotropy ratio of 23 is predicted for a COF formed from linker91 as the molecular building block (see Figure 1) with the hof topology (the schematic of which is shown in Figure S29, Supporting Information).

The minimum and maximum thermal conductivities along the different directions for the anisotropic COFs are shown in Figure 2d. Most notably, the highest thermal conductivity predicted in a particular direction reaches as high as 47 W m<sup>-1</sup> K<sup>-1</sup>. This is comparable to the thermal conductivity of several fully dense inorganic solids such as GaAs.<sup>[74]</sup> As such, these COFs mark a new regime of materials design that combines low densities with high thermal conductivities (see Figure S3, Supporting Information). Moreover, 38 COFs possess maximum thermal conductivity ( $\kappa_{\rm max}$ ) greater than 5 W m $^{-1}$  K $^{-1}$  along one direction (see Table S3, Supporting Information for the details of their physical attributes) and among these COFs, 14 COFs (whose schematics are shown in Figures S16-S28, Supporting Information) possess  $\kappa_{\rm max} > 10 \text{ W m}^{-1} \text{ K}^{-1}$  (Figure 2e). Most notably, all 14 COFs have linker91 as the organic building block (Figure 1a), thus forming another criterion (along with the necessity of the carbon-carbon linkage) for achieving high thermal conductivities in COFs.

Another aspect worth noting is that the anisotropy ratios of these COFs increase with increasing thermal conductivity and are considerably higher for structures with intermediate (that is in the range of 0.2–1 W  $m^{-1}$  K<sup>-1</sup>) and high (>1 W  $m^{-1}$  K<sup>-1</sup>) thermal conductivity (as shown in the inset of Figure 2e). This can be mainly attributed to the differences in the alignment of the polymeric chains along the three principal directions, where heat flow is better facilitated if the polymeric chains are better aligned along that direction (see Figure 2c). Similar conclusion was also made for MOFs<sup>[38,52]</sup> and for interpenetrated COF-300.<sup>[59]</sup> In fact,

and-conditions) on Wiley Online Library for rules of use; OA articles are governed by the applicable Creative Comn-

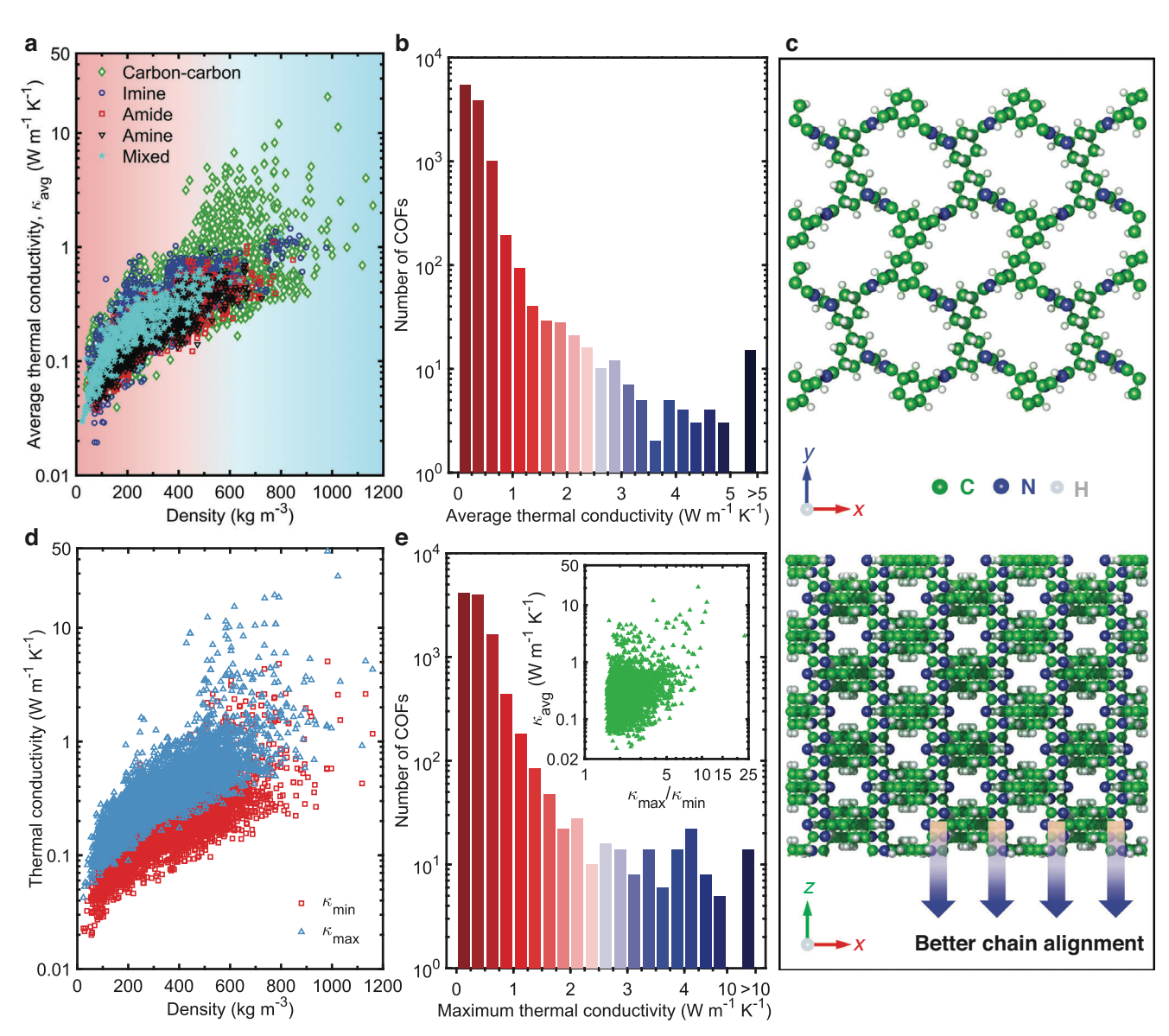


Figure 2. a) Average thermal conductivity values of 10,750 COFs categorized based on their bond types. Overall, structures with carbon–carbon bonds as their linkage chemistries exhibit both high densities and higher thermal conductivity values compared to COFs with other bonding linkages. b) The distribution of average thermal conductivity values for the 10,750 COFs, with a bin size of 0.25 W m<sup>-1</sup> K<sup>-1</sup>. Notably, we observe that 97% of the structures have average thermal conductivity values below 1 W m<sup>-1</sup> K<sup>-1</sup>, while 15 structures exhibit  $κ_{avg}$  greater than 5 W m<sup>-1</sup> K<sup>-1</sup>. c) Schematic illustration of the highest thermal conductivity COF, highlighting its anisotropic structure and better alignment of the polymeric chains along the z-direction with κ=47 W m<sup>-1</sup> K<sup>-1</sup>. d) Maximum and minimum thermal conductivities as a function of density for 3,748 anisotropic COFs with thermal conductivity anisotropy ratio of ≥1.5. e) The distribution of maximum thermal conductivity values for the 10,750 COFs. Note, the bin size after 4 W m<sup>-1</sup> K<sup>-1</sup> is 2 W m<sup>-1</sup> K<sup>-1</sup>. We found 14 structures that have  $κ_{max}$  greater than 10 W m<sup>-1</sup> K<sup>-1</sup>. (inset) Average thermal conductivity of anisotropic COFs as a function of their anisotropy ratio, which range from a minimum of 1.5 to a maximum of 23 and is generally higher for higher thermal conductivity COFs.

in a recent work by Islamov et al., [38] where they performed similar high-throughput calculations of  $\kappa$  on a hypothetical dataset of 10,194 MOFs, chain alignment of the organic linkers along the heat flow direction was also found to lead to six MOFs with  $\kappa_{\rm avg}>10~{\rm W~m^{-1}~K^{-1}}$ . We note that while the number of parallel and perpendicular bonded interactions along each direction might also influence the phonon dynamics, leading to variations in thermal conductivity along that direction, the complex structural topologies and node configurations of COFs requires a de-

tailed investigation to segregate the influence of bonded interactions on the heat conduction along each principal direction and therefore deserves further investigation.

As mentioned above, density alone cannot account for the wide range of thermal conductivities spanning 0.02 to 50 W m $^{-1}$  K $^{-1}$  that we predict for the 10,750 3D COF structures. Therefore, we investigate the impact of various internal structural parameters and their optimized combinations on the thermal conductivity of COFs. To this end, we plot  $\kappa_{\rm max}$  against LPD, void fraction, and

www.small-journal.com

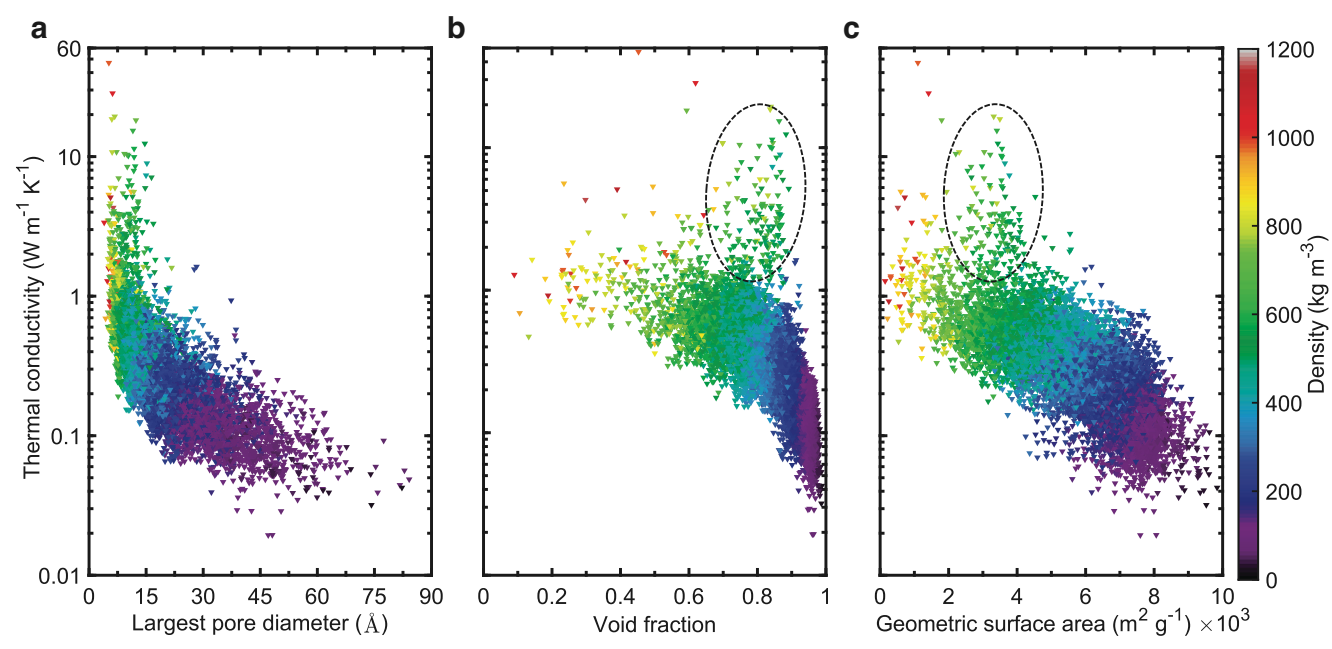


Figure 3. Thermal conductivity as a function of (a) void fraction, (b) largest pore diameter, and (c) geometric surface area, color-mapped according to their density. Most of the COFs with thermal conductivity  $> 1 \text{ W m}^{-1} \text{ K}^{-1}$  possess void fractions in the range of 0.6–0.9 and GSA values of 2,000–4,000 m<sup>2</sup> g<sup>-1</sup>.

GSA, as shown in Figure 3a-c. Not surprisingly, we observe a decrease in thermal conductivity with an increase in pore diameter (Figure 3a), aligning well with prior studies on COFs that have demonstrated higher thermal conductivities by reducing pore size and limiting vibrational scattering at the pore walls.[25,39,58] More specifically, we find that COFs with relatively high thermal conductivity ( $\kappa > 1 \text{ W m}^{-1} \text{ K}^{-1}$ ) tend to have LPD values smaller than 15 Å (Figure 3a). The more interesting (and surprising) observations are formulated when we consider the impact of void fraction and available GSA on  $\kappa$ . As shown in Figure 3b, all COFs with void fractions greater than 0.9 exhibit  $\kappa$  <0.25 W m<sup>-1</sup> K<sup>-1</sup>, which is expected since large void fractions correspond to low densities and high porosities. Thus, given the fact that high densities are directly related to lower void fractions, it can be expected that lower void fractions result in higher thermal conductivity values. We find, however, that the majority of COFs with  $\kappa > 1$  W m<sup>-1</sup> K<sup>−1</sup> (as highlighted in Figure 3b) possess void fractions in the range of 0.6 to 0.9, corresponding to COF densities in the range of approximately 500 to 900 kg m<sup>-3</sup>. Similarly, COFs with GSA in the range of approximately 2,000 to 4,000 m<sup>2</sup> g<sup>-1</sup> (Figure 3c) contain the largest number of COFs that have high  $\kappa$  values. Therefore, the design of 3D COFs with exceptionally high thermal conductivity requires an intricate balance between the choices for the values of their density, void fraction, and GSA that need to be within the specified ranges, which we explore in more detail in the following discussions.

In general, COFs with larger pores are associated with lower densities. As such, the combination of high densities with large pore sizes is not typical for porous materials. Therefore, to optimize these parameters for achieving the desired thermal conductivity in COFs, we plot the thermal conductivity as a function of the product of LPD and density, as shown in **Figure 4**a–d. We find that thermal conductivity is at the lower end for high and

low values of LPD×density. An optimum range of 4 to 8 Å g cm<sup>-3</sup> is associated with the most number of COFs with  $\kappa > 1$  W m<sup>-1</sup> K<sup>-1</sup>. This optimal range, however, is not sufficient to ensure high  $\kappa$  values since many COFs with ultralow  $\kappa$  also possess LPD×density in the range of 4 to 8 Å g cm<sup>-3</sup> (specifically, those with LPD>40 Å, density<300 kg m<sup>-3</sup>, void fraction>0.9, and GSA>6,000 m² g<sup>-1</sup>, as shown in Figure 4a–d). Thus, for 3D COFs to achieve high  $\kappa$ , several structural properties must align, including LPD<15 Å (Figure 4a), void fractions in the range of 0.6 to 0.9 (Figure 4b), GSA<4,000 m² g<sup>-1</sup> (Figure 4c), and density in the range of ≈500 to 900 kg m<sup>-3</sup> (Figure 4d).

Figure 4d highlights different regions of the COF structureproperty space that are worth describing in more detail. In region 1, COFs have low densities ( $<50 \text{ kg m}^{-3}$ ) and large pores (>50 Å), which ensures that  $\kappa$  is very low (<0.05 W m<sup>-1</sup> K<sup>-1</sup>). These ultralow values of  $\kappa$  can be ascribed to considerable vibrational scattering at the huge pores and low areal densities of covalent bonds which are crucial in dictating the heat conduction in these porous polymeric frameworks (see Figure 4e for representative schematic of a COF from this region). In region 2, the reduction in the LPD, void fraction, and GSA, along with the densification of the COF framework (with higher areal densities of bonded interactions as schematically shown in Figure 4f) lead to an order of magnitude increase in  $\kappa$  ( $\approx 0.75 \text{ W m}^{-1} \text{ K}^{-1}$ ). Region 3 corresponds to COFs with the highest  $\kappa$  (>10 W m<sup>-1</sup> K<sup>-1</sup>), which can mainly be ascribed to highly aligned polymer chains along the heat flow direction, yet the areal densities of covalent bonds are not as high as that of Region 4 with relatively lower  $\kappa$  values (see Figure 4g,h for representative schematics of COFs from regions 3 and 4, respectively). Note, region 4 has lower void fractions and higher densities as compared to region 3. This is an important conclusion in terms of the design of COFs with high thermal conductivities, since higher areal densities of bonded interactions

www.small-journal.com

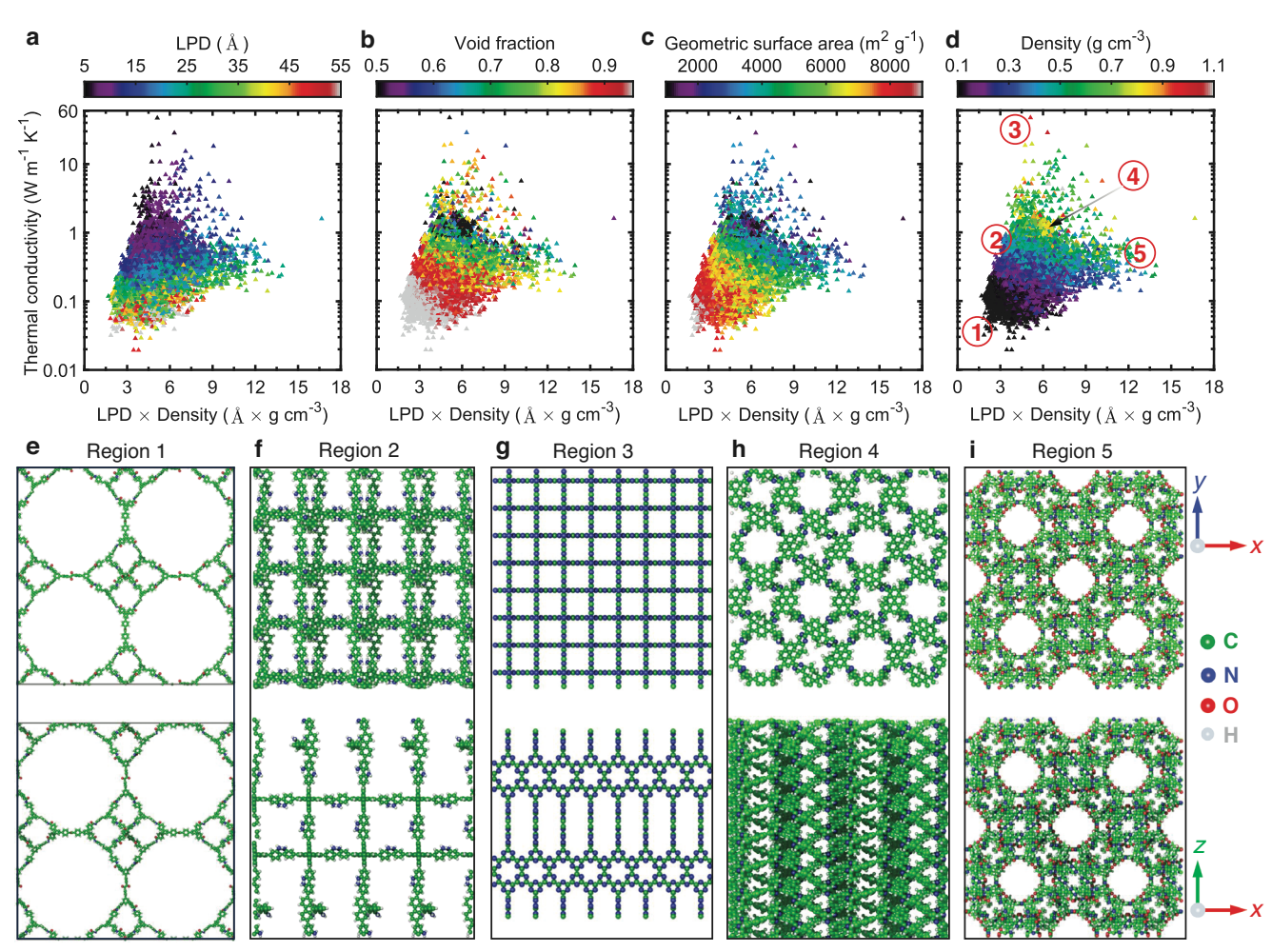


Figure 4. Thermal conductivity as a function of the product of the largest pore diameter (LPD) and density, color-mapped by a) LPD, b) void fraction, c) geometric surface area, and d) density. Schematic illustrations of COF structures from different regions shown in Figure 4d. e) Region 1: very low density and very high LPD. f) Region 2: average density and low LPD. g) Region 3: high density and low LPD with well-aligned polymer chains along the heat flow direction. h) Region 4: high density and low LPD. The polymer chains are not as well-aligned as region 3. i) Region 5: average density and high LPD.

does not always lead to high  $\kappa$ , as would be expected if density was the sole structural parameter determining  $\kappa$ . Finally, in region 5, as LPD is relatively higher ( $\approx$ 25 Å) compared to the other three regions (2, 3, and 4), which have LPD values <15 Å, and while the densities and void fractions stay comparable to that in region 2, we observe a substantial drop in  $\kappa$ . Again, even though the areal density of bonded interactions are similar to region 4 (see Figure 4i), the large pores (that are  $\approx$ 3 times bigger) result in considerable vibrational scattering, thus lowering  $\kappa$  by  $\approx$ 4 times in comparison to region 4. Taken together, our assertion that density alone does not satisfy the criteria for dictating  $\kappa$  is reemphasized, since these discussions highlight the importance of pore size and chain alignment in driving high  $\kappa$  for these 3D COFs.

So far, we have mainly focused on achieving high thermal conductivities in COFs. In what follows, we will attempt to explain how ultralow thermal conductivities can be attained for COFs. In this regard, we note here that the lowest reported thermal conductivity for any fully dense solid was measured for the fullerene derivative PCBM with a value of approximately  $0.05~\mathrm{W}~\mathrm{m}^{-1}~\mathrm{K}^{-1}.^{[75,76]}~\mathrm{We}~\mathrm{find}~94~\mathrm{COFs}$  with comparable to or lower thermal conductivities than that of PCBM, albeit with very low densities (that are  $\leq 150 \text{ kg m}^{-3}$ ). While our results suggest that achieving thermal conductivities on par with PCBM for COFs with densities greater than 200 kg m<sup>-3</sup> is challenging, our high-throughput screening has unveiled a distinctive descriptor for COFs, leading to comparatively low thermal conductivity even when the COF density exceeds 200 kg m<sup>-3</sup> (see Figure 5). Specifically, COFs containing either silicon or sulfur atoms in their extended periodic structure exhibit relatively lower thermal conductivities. We can attribute this to the mass and bond disorders and more importantly to the mismatch in the vibrational frequency spectrum due to the introduction of the heavier atoms in the extended COF frameworks. Typically, COFs are formed by lighter atoms, namely carbon, nitrogen, and boron, and so the heavier silicon and sulfur atoms can introduce significant mass and bond disorders resulting in additional vibrational scattering. Similar observations have also been made for MOFs, where large mass mismatches resulting from the

\_\_\_small

www.small-journal.com

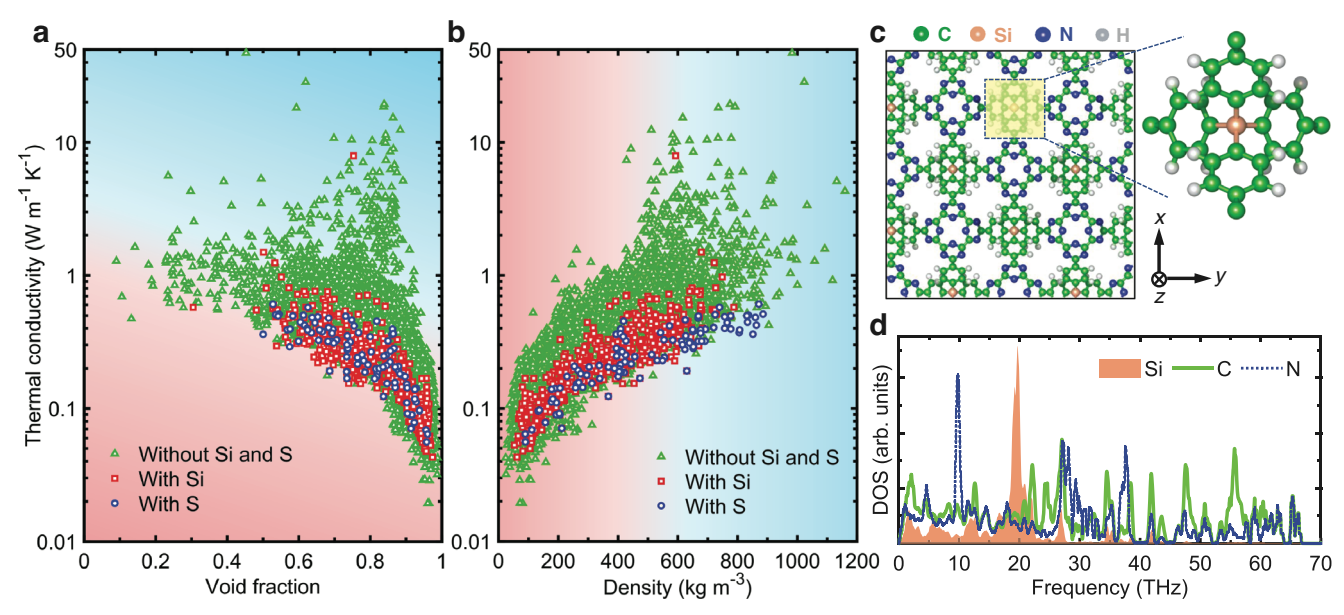


Figure 5. Comparison of average thermal conductivity values for structures with and without silicon or sulfur atoms as a function of (a) void fraction and (b) density. c) Schematic illustration of a representative COF structure with silicon atoms in the linkers. The silicon or sulfur atoms, which are heavier than carbon, nitrogen or boron, add additional vibrational scattering through mass and bond disorders. d) Vibrational density of states for the representative COF structure with silicon atoms, highlighting the mismatch in the phonon spectrum of the heavier atom with respect to the lighter carbon and nitrogen atoms.

heavier metallic nodes have shown to substantially reduce their thermal conductivity. [38,46,66] The vibrational mismatch for a representative COF with silicon incorporated in the linker (as shown in the schematic in Figure 5c) is quantified by comparing the vibrational density of states associated with silicon atoms as compared to that of the lighter carbon and nitrogen atoms (Figure 5d). Our calculations show that the silicon atoms are associated with a narrower frequency spectrum compared to carbon and nitrogen atoms with more than twice the vibrational frequency ranges. This leads to reduced overlap in the phonon spectrum associated with the lighter and heavier atoms, thus increasing phonon scattering and ultimately resulting in reduced thermal conductivities.

From the discussions above, it is apparent that large pores and low densities result in COFs with ultralow thermal conductivities. While materials with highly porous structures and low thermal conductivities are typically of interest for applications such as thermal insulation in buildings and refrigerators, for other specific technological needs, such as in thermoelectrics and thermal barrier coatings, it is desirable to utilize dense solids.[77–79] We have identified COFs with silicon and sulfur atoms in the linkers to possess low thermal conductivities ( $\approx 0.2 \text{ W m}^{-1} \text{ K}^{-1}$ ) even at relatively higher densities. However, we have not fully considered the effect of other structural parameters in driving low  $\kappa$  values in COFs, especially at relatively higher densities. To this end, as 97% of the COFs have  $\kappa_{\rm avg}$  below 1 W m $^{-1}$  K $^{-1}$ , we employ a binning approach to reveal their relationships between  $\kappa$  and the structural parameters that we have considered in our earlier discussions (see Figure 6; Figure S10, Supporting Information). In general, we observe a consistent trend of decreasing thermal conductivity with increasing pore diameter, void fraction, and GSA for these low thermal conductivity COFs. More specifically,

for COFs with  $\kappa_{\rm avg}$  <0.2 W m<sup>-1</sup> K<sup>-1</sup>, we note LPD values>27 Å, void fraction>0.9, and GSA>7,000 m<sup>2</sup> g<sup>-1</sup>. Furthermore, as highlighted in Figure 6a, we can achieve  $\kappa_{\rm avg}$  <0.2 W m<sup>-1</sup> K<sup>-1</sup> at a relatively high density of ≈350 kg m<sup>-3</sup> through the inclusion of silicon or sulfur in the linkers, and frameworks with average LPD of ≈31 Å, average void fraction of ≈0.82, and average GSA of ≈4,800 m<sup>2</sup> g<sup>-1</sup>.

Since COFs are a class of polymeric materials, it is also noteworthy that we find 1,219 COFs with  $\kappa_{\rm avg} \leqslant 0.1~{\rm W~m^{-1}~K^{-1}},$  comparable to or even lower than typical polymers. [77] These COFs have average LPD of  $\approx 36~{\rm \AA}$ , average void fraction of  $\approx 0.94$ , and average GSA of  $\approx 7,432~{\rm m^2~g^{-1}}.$  Within this subset, the 94 COFs that we identified earlier with  $\kappa_{\rm avg} \leqslant 0.05~{\rm W~m^{-1}~K^{-1}},$  possess average density of  $\approx 76~{\rm kg~m^{-3}},$  average LPD of  $\approx 50~{\rm \AA},$  average void fraction of  $\approx 0.96,$  and average GSA of  $\approx 7,825~{\rm m^2~g^{-1}}$  (see Table S4, Supporting Information for the details of their physical attributes). This comprehensively and quantitatively demonstrates that to achieve COFs with exceptionally low thermal conductivities, they need to possess very large pores, high void fractions, and extensive surface areas.

While thermal transport is an important consideration, in most applications of COFs, the storage capacity for infiltrated guest species is of primary concern for choosing the right combination of the structural parameters. Therefore, it is instructive to assess the interplay between deliverable capacity (which is a quantitative measure of gas storage capacity) and the structural parameters we have considered so far. To delve into this relationship, we take the deliverable capacity of methane gas as calculated in Ref. [71] via grand-canonical Monte Carlo simulations performed on the same COF database. Further details regarding the calculation of deliverable capacities can be found in Ref. [71]

www.small-journal.com

LPD  $\times$  Density ( $^{\text{A}} \times \text{g cm}^{-3}$ )

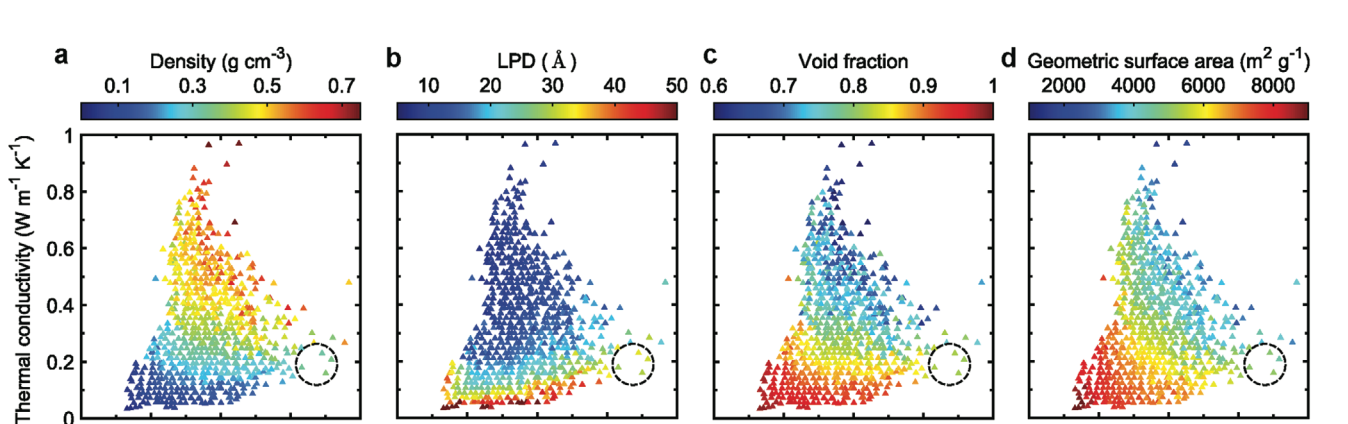


Figure 6. Average thermal conductivity of COFs below 1 W  $m^{-1}$  K<sup>-1</sup> as a function of the product of the largest pore diameter (LPD) and density, colormapped by (a) density, (b) LPD, (c) void fraction, and (d) geometric surface area. For clarity, each plot is discretized into 60 × 60 bins, representing the average property of the COFs in that bin.

LPD  $\times$  Density ( $^{\text{A}} \times \text{g cm}^{-3}$ )

12 0 3

LPD  $\times$  Density ( $^{\text{A}} \times \text{g cm}^{-3}$ )

In their work, Mercado et al.[71] uncovered an intriguing trend in deliverable capacity of these COFs (as shown in Figure 7a-c), revealing an initial increase with density that reaches its maximum for structures in the density range of 400 to 600 kg m<sup>-3</sup>. Beyond 600 kg m<sup>-3</sup>, a substantial decrease in deliverable capacity was observed, emphasizing that structures with the highest deliverable capacities are confined to a narrow density range. Similar to the wide variation found in thermal conductivity for a specific density (Figure 2), a broad variation was also observed in deliverable capacity at constant density. For example, at a constant density of 400 kg m<sup>-3</sup>, many structures were shown to have low deliverable capacities (less than 135  $v_{STP}/v$ ). While structures with high pore diameter and GSA are expected to have high storage capacity, it is surprising that structures with high LPD, high void fraction, and high GSA were found to have significantly low deliverable capacity (less than 100 v<sub>STP</sub>/v) (Figure 7a-c). Interestingly, a majority of COFs with LPD in the range of 10 to 15 Å, void fraction in the range of 0.8 to 0.9, and GSA in the range of 3,500 to 6,000  $m^2 g^{-1}$  were found to exhibit deliverable capacities greater than 180  $v_{STP}/v$ , which correlates well with the range of values that we have prescribed for COFs to possess high thermal conductivities, a trait highly desirable for efficient heat dissipation during gas loading.

12 0

LPD  $\times$  Density ( $^{\text{A}} \times \text{g cm}^{-3}$ )

Therefore, to quantify the relationship between the two important physical traits for COFs (namely, their thermal conductivity and gas adsorption capacity) for gas storage applications, we consider deliverable capacity for methane as a function of the thermal conductivity of the COFs, as shown in Figure 7. We observe an interesting relationship between the deliverable capacity and the thermal conductivity, where the deliverable capacities initially increase with increasing thermal conductivity reaching maximum values followed by a sharp decrease. Fortuitously, COFs with high deliverable capacities (>180  $v_{STP}/v$ ) also possess relatively higher thermal conductivities (in the range of 0.2 to 1 W m<sup>-1</sup> K<sup>-1</sup>), as shown in Figure 7. It is worth noting here that similar to the results of our high-throughput thermal conductivity, it was found that carbon-carbon bonded 3D COFs have the largest percentage of promising structures in terms of high deliverable capacities.[71]

The largest percentage of COFs with lower deliverable capacities are mainly associated with thermal conductivities lower than 0.2 W m<sup>-1</sup> K<sup>-1</sup> (which is not surprising as these COFs possess very low densities as shown in Figure 7d). However, COFs with relatively higher thermal conductivities (>0.5 W m<sup>-1</sup> K<sup>-1</sup>) can also possess low deliverable capacities. This is because these COFs have nominally small LPD and GSA values (Figures 7e,f) that are not ideal for gas storage applications. Notably, we find 31 COFs with deliverable capacities greater than 180  $v_{STP}/v$  (on par with some of the highest experimentally determined values for COFs)[12,71] and thermal conductivities exceeding 1 W m<sup>-1</sup> K<sup>-1</sup> and reaching as high as 12.4 W m<sup>-1</sup> K<sup>-1</sup> (see Table \$2, Supporting Information for the details of their physical attributes). These COFs have average density of ≈475 kg m<sup>-3</sup>, average LPD of ≈14.2 Å, average void fraction of ≈0.86, and average GSA of  $\approx 4,100$  m<sup>2</sup> g<sup>-1</sup>. Therefore, for gas storage applications, the ideal COF structures with relatively high thermal conductivities should be designed with strategic combinations of optimal LPD, density and GSA values, as we have reported.

12

## 3. Conclusion

Our extensive high-throughput thermal conductivity calculations for 10,750 different COFs provide valuable insights into their structure-property relationships; a concise summary and recommended design strategies for achieving either high or low thermal conductivities in 3D COFs is presented in Table 1. Along with identifying key structural and chemical features that can be modulated to tune their thermal conductivity over three orders of magnitude, we also identify 31 COFs with high methane uptakes (>180 v<sub>STP</sub>/v) and relatively high thermal conductivities  $(\gtrsim 1 \text{ W m}^{-1} \text{ K}^{-1})$ . Porous framework materials demonstrating such a combination of properties are immensely desirable for gas storage applications, where the exothermic adsorption processes come with the prerequisite for proper heat dissipation capabilities. We hope that the design strategies presented in this work can provide valuable guidelines for the synthesis of COFs with targeted thermal properties. However, for COFs to fulfill their potential in practical applications, they need to combine a host of

conditions) on Wiley Online Library for rules of use; OA articles are governed by the applicable Creative C

www.small-journal.com

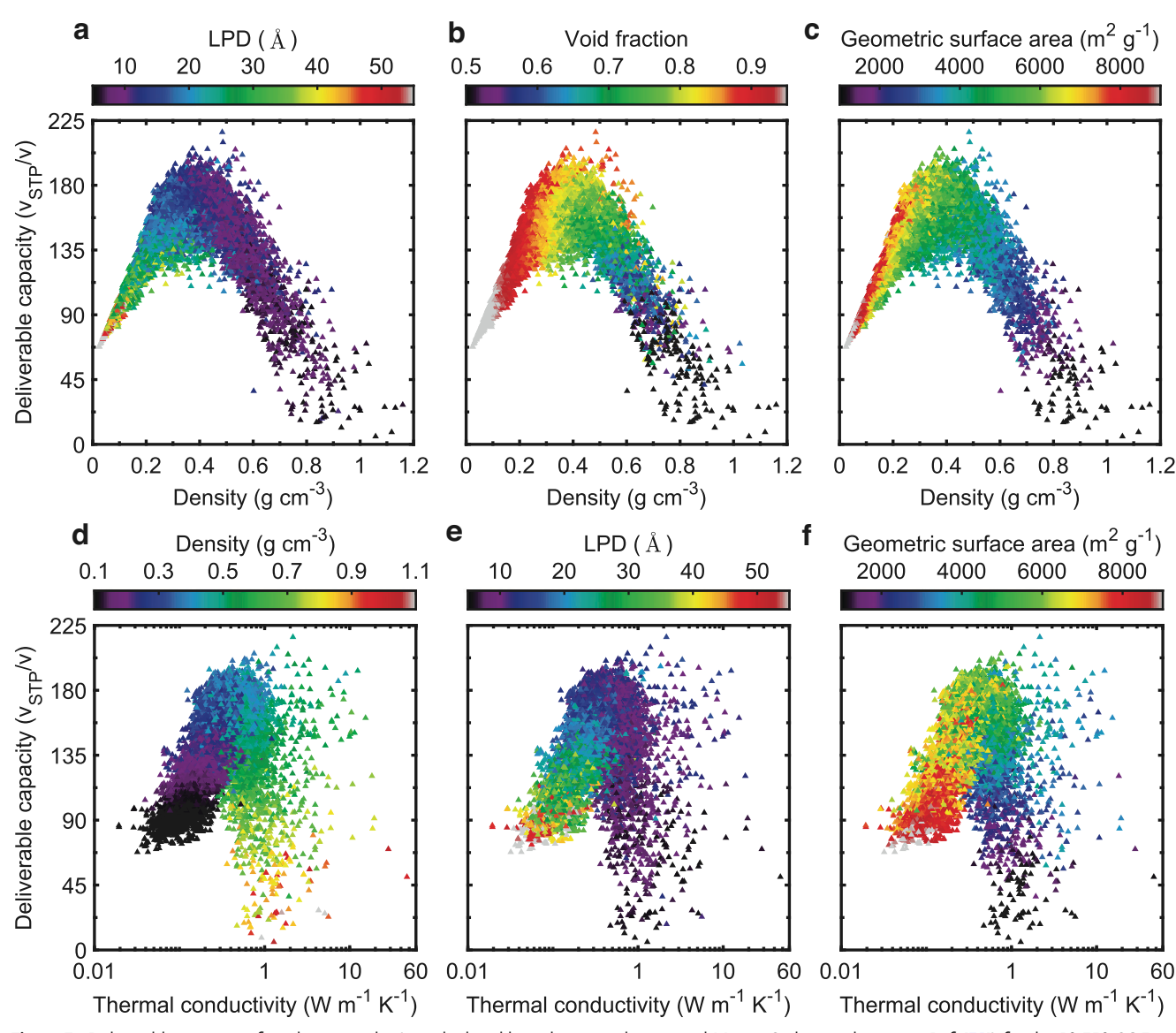


Figure 7. Deliverable capacity of methane uptake (as calculated based on grand-canonical Monte Carlo simulations in Ref. [71]) for the 10,750 COFs as a function of the density, color-mapped by (a) largest pore diameter (LPD), (b) void fraction, and (c) geometric surface area. Deliverable capacity as a function of the calculated maximum thermal conductivity values, color-mapped by (d) density, (e) LPD, and (f) geometric surface area.

material properties including 'user-defined' thermal conductivity, which will ultimately help position them as multifunctional materials for the next generation of technologies.

# 4. Computational Methods Section

Our COF structures were taken from the Materials Cloud platform, which had a total of 69,840 COFs.<sup>[71]</sup> From this database, 12,000 structures were carefully selected to ensure the inclusion of COFs spanning the entire density range for each of the four bond types. Due to the limited number of high-density structures, all COFs were included with densities greater than 400 kg m<sup>-3</sup> for amide, amine, and mixed bond types. Since the structures with carbon–carbon and imine bond types had relatively higher densities, all structures were included with these bond

types that had densities greater than 500 kg  $\rm m^{-3}$ . Out of the 12,000 COFs, converged thermal conductivities were obtained for 10,750 structures.

For the MD simulations, the Large-scale Atomic Molecular Massively Parallel Simulator (LAMMPS) package was employed. [80] Recent studies have highlighted potential discrepancies in the calculation of heat flux as implemented in LAMMPS, particularly in systems with many-body interactions. [81,82] Therefore to ensure the accuracy of thermal conductivity predictions for COF structures, the version of LAMMPS was utilized that implements the centroid atomic stress formulation, ensuring the correct computation of heat flux for the COFs. [83] Notably, to describe the bonded interactions between the atoms, the Universal Force Field (UFF) modified for porous organic frameworks was utilized. [84,85] The force





**Table 1.** Summary of strategies for tailoring COFs with low/high thermal conductivities.

#### For high thermal conductivity

The design strategies to achieve high  $\kappa$  in COFs include:

- Using densities greater than 500 kg m<sup>-3</sup>
- Using structures with small pores (less than 15 Å) and low GSA ( $\lesssim$ 4,000 m<sup>2</sup> g<sup>-1</sup>)
- Maintaining nominal void fractions in the range of  $\approx 0.6-0.9$
- Ensuring highly aligned polymeric chains along the heat flow direction
- Incorporating carbon-carbon linkages for the bond-formation chemistry
- Using linkers that facilitate heat transfer, such as linker91 and linker92 as the organic building block (see Figure 1a)

#### For low thermal conductivity

The design strategies to attain low  $\kappa$  in COFs include:

- Using structures with large pores (>36 Å)
- Using high void fractions (>0.9) and high GSA (>7,000  $m^2$   $g^{-1}$ )
- Utilizing linkers with polymeric chains that are not well-aligned with the direction of heat flow
- Utilizing molecular building blocks containing heavier atoms (e.g., silicon or sulfur)

field parameters include terms for bond, angle, dihedral, and torsional interactions, with no charges considered, and a non-bonding interaction cutoff set at 12.5 Å. We note that electrostatic interactions were not included in the calculations due to the high computational cost.

The computational domains were initially equilibrated under the N-V-T ensemble for 1.5 ns with a timestep of 0.5 fs where the number of particles, volume, and temperature were kept constant. Note, periodic boundary conditions were used in all three directions for all the simulations. Furthermore, an additional equilibration was conducted under N-V-E ensemble for 1 ns where the number of particles, volume and total energy of the system remain constant. Following the equilibration steps, the Green-Kubo (GK) formalism was employed within the framework of equilibrium molecular dynamics (EMD) simulations to compute the thermal conductivities of the computational domains. In the GK formalism, the thermal conductivity along the  $\alpha^{\text{th}}$  direction is given as,

$$\kappa_{\alpha} = \frac{1}{k_{\rm B} V T^2} \int_0^{\infty} \langle J_{\alpha}(t) J_{\alpha}(0) \rangle dt \tag{1}$$

here, t represents time, T and V are the temperature and volume of the system, and term  $\langle J_{\alpha}(t)J_{\alpha}(0)\rangle$  denotes the  $\alpha^{\text{th}}$  component of the heat current autocorrelation function (HCACF), expressed as, [86]

$$J = \frac{1}{V} \left( \sum_{i} \nu_{i} \varepsilon_{i} + \sum_{i} S_{i} \cdot \nu_{i} \right)$$
 (2)

here,  $v_i$ ,  $\varepsilon_i$ , and  $S_i$  represent the velocity, energy and stress of atom i, respectively. The total correlation time, ranging from 5 to 75 ps depending on COF density (with shorter times for low-density COFs and longer times for high-density COFs) was utilized. Heat current was calculated every 7 fs during the data collection period

followed by integration of the heat current to determine the converged thermal conductivities. The calculations were performed under the microcanonical ensemble for a total of 4.5 ns. For convergence of thermal conductivity with domain size, additional simulations were run for various structures at different densities with a range of domain sizes. Thus, it was ensured that the chosen lengths that exceed 50 Å for all the COFs in a certain direction were sufficient to avoid size-effects in the thermal conductivity calculations. [87] We also note that the reported thermal conductivities of the 10,750 3D COF structures were determined based on the average of five independent simulations. Further details regarding the GK formalism can be found in the Supporting Information.

For some COFs, non-decaying oscillatory behavior was observed in the instantaneous thermal conductivity, making it difficult to obtain converged thermal conductivity values with the GK approach for such cases. Therefore, for accurate thermal conductivity predictions, an adaptive algorithm was developed similar to the automated thermal conductivity extraction algorithm developed by Islamov et al.[38] The algorithm involves the computation of the mean, standard deviation, and slope obtained from the linear fit to the instantaneous thermal conductivity values at certain correlation times. To determine the correlation time interval where converged (and plateaued) thermal conductivity can be obtained, the algorithm calculates the slope of the linear fit for data segments of 3 ps in length at 2 ps increments when the total correlation time is ≤15 ps. For total correlation time exceeding 15 ps, the algorithm employs segments of 15 ps length at 5 ps increments. The calculated slope was then normalized with the mean of the instantaneous thermal conductivity.

Finally, the algorithm checks whether any linear segment has standard deviation less than 20 percent of the mean of the instantaneous thermal conductivity and a normalized slope less than 0.01 ps<sup>-1</sup>. If a single data segment satisfies the criteria, that interval is accepted. In cases where multiple segments meet the criteria, they are sorted based on standard deviations, and preference is given to the segment with the lowest standard deviation. Moreover, when comparing segments with equal standard deviations, priorioty is given to the segment with the lower slope. Structures failing to meet these conditions were filtered out, and subsequent simulations were rerun with an increased correlation time. Given the large number of COFs screened, this process was automated ensuring robust calculations by systematically eliminating unconverged values.

The density of the COF structures were determined using the LAMMPS package.<sup>[80]</sup> The calculations of other structural properties such as pore sizes, void fractions, and geometric surface areas were obtained from the work of Mercado et al.,<sup>[71]</sup> where pore sizes, and geometric surface areas were computed using Zeo++,<sup>[88]</sup> and the void fraction was determined by probing the framework with a helium molecule using the Widom particle insertion method.<sup>[89,90]</sup> For further details regarding the calculation of geometric properties, please refer to Ref. [71].

# **Supporting Information**

Supporting Information is available from the Wiley Online Library or from the author.

\_\_\_\_\_5111U1

www.small-journal.com

# Acknowledgements

This work was supported by the Office of Naval Research, Grant no. N00014-21-1-2622. The work is also partially supported by the National Science Foundation (NSF Award no. 2119365).

## **Conflict of Interest**

The authors declare no conflict of interest.

## **Data Availability Statement**

The data that support the findings of this study are available from the corresponding author upon reasonable request.

## Keywords

covalent organic frameworks, design strategy, high-throughput calculation, structure-property relationships, thermal conductivity

Received: March 4, 2024 Revised: March 8, 2024 Published online:

- [1] K. Geng, T. He, R. Liu, S. Dalapati, K. T. Tan, Z. Li, S. Tao, Y. Gong, Q. Jiang, D. Jiang, Chem. Rev. 2020, 120, 8814.
- [2] A. P. Cote, A. I. Benin, N. W. Ockwig, M. O'Keeffe, A. J. Matzger, O. M. Yaghi, *Science* 2005, 310, 1166.
- [3] F. J. Uribe-Romo, J. R. Hunt, H. Furukawa, C. Klock, M. O'Keeffe, O. M. Yaghi, J. Am. Chem. Soc. 2009, 131, 4570.
- [4] J. L. Mendoza-Cortés, S. S. Han, H. Furukawa, O. M. Yaghi, W. A. Goddard III, J. Phys. Chem. A 2010, 114, 10824.
- [5] P. J. Waller, F. Gándara, O. M. Yaghi, Acc. Chem. Res. 2015, 48, 3053.
- [6] C. S. Diercks, O. M. Yaghi, Science 2017, 355, eaal 1585.
- [7] C. Qian, L. Feng, W. L. Teo, J. Liu, W. Zhou, D. Wang, Y. Zhao, *Nat. Rev. Chem.* 2022, 6, 881.
- [8] M.-X. Wu, Y. Wang, G. Zhou, X. Liu, Coord. Chem. Rev. 2021, 430, 213735.
- [9] J. L. Mendoza-Cortes, T. A. Pascal, W. A. Goddard III, J. Phys. Chem. A 2011, 115, 13852.
- [10] S. S. Han, H. Furukawa, O. M. Yaghi, W. A. Goddard Iii, J. Am. Chem. Soc. 2008, 130, 11580.
- [11] M. S. Lohse, T. Bein, Adv. Funct. Mater. 2018, 28, 1705553.
- [12] H. Furukawa, O. M. Yaghi, J. Am. Chem. Soc. 2009, 131, 8875.
- [13] S. Amirjalayer, R. Q. Snurr, R. Schmid, J. Phys. Chem. C 2012, 116, 4921.
- [14] S. Xu, H. Sun, M. Addicoat, B. P. Biswal, F. He, S. Park, S. Paasch, T. Zhang, W. Sheng, E. Brunner, Y. Hou, M. Richter, X. Feng, *Adv. Mater.* 2021, 33, 2006274.
- [15] M. Liu, J. Liu, K. Zhou, J. Chen, Q. Sun, Z. Bao, Q. Yang, Y. Yang, Q. Ren, Z. Zhang, Adv. Sci. 2021, 8, 2100631.
- [16] X. Hu, Z. Zhan, J. Zhang, I. Hussain, B. Tan, Nat. Commun. 2021, 12, 6596.
- [17] C. Xia, K. O. Kirlikovali, T. H. C. Nguyen, X. C. Nguyen, Q. B. Tran, M. K. Duong, M. T. N. Dinh, D. L. T. Nguyen, P. Singh, P. Raizada, V.-H. Nguyen, S. Y. Kim, L. Singh, C. C. Nguyen, M. Shokouhimehr, Q. V. Le, Coord. Chem. Rev. 2021, 446, 214117.
- [18] P. She, Y. Qin, X. Wang, Q. Zhang, Adv. Mater. 2022, 34, 2101175.
- [19] D. Yan, Z. Wang, P. Cheng, Y. Chen, Z. Zhang, Angew. Chem. 2021, 133, 6120.

- [20] Y. Shi, J. Yang, F. Gao, Q. Zhang, ACS Nano 2023, 17, 1879.
- [21] M.-X. Wu, Y.-W. Yang, Chin. Chem. Lett. 2017, 28, 1135.
- [22] L. Wang, B. Dong, R. Ge, F. Jiang, J. Xu, ACS Appl. Mater. Interfaces 2017, 9, 7108.
- [23] B. Huang, A. McGaughey, M. Kaviany, Int. J. Heat Mass Transfer 2007, 50. 393.
- [24] B. Huang, Z. Ni, A. Millward, A. McGaughey, C. Uher, M. Kaviany, O. Yaghi, Int. J. Heat Mass Transfer 2007, 50, 405.
- [25] M. A. Rahman, C. J. Dionne, A. Giri, ACS Appl. Mater. Interfaces 2022, 14. 21687.
- [26] A. Giri, A. M. Evans, M. A. Rahman, A. J. McGaughey, P. E. Hopkins, ACS Nano 2022, 16, 2843.
- [27] S. K. Freitas, R. S. Borges, C. Merlini, G. M. Barra, P. M. Esteves, J. Phys. Chem. C 2017, 121, 27247.
- [28] S. S. Han, J. L. Mendoza-Cortés, W. A. Goddard Iii, Chem. Soc. Rev. 2009, 38, 1460.
- [29] J. Xu, Y. He, S. Bi, M. Wang, P. Yang, D. Wu, J. Wang, F. Zhang, Angew. Chem. 2019, 131, 12193.
- [30] X. Li, K. Zhang, G. Wang, Y. Yuan, G. Zhan, T. Ghosh, W. P. Wong, F. Chen, H.-S. Xu, U. Mirsaidov, K. Xie, J. Lin, K. P. Loh, *Nat. Synth.* 2022, 1, 382.
- [31] J. Lin, Y. Zhong, L. Tang, L. Wang, M. Yang, H. Xia, Nano Select 2022, 3, 320.
- [32] J. Wieme, S. Vandenbrande, A. Lamaire, V. Kapil, L. Vanduyfhuys, V. Van Speybroeck, ACS Appl. Mater. Interfaces 2019, 11, 38697.
- [33] H. Babaei, M. E. DeCoster, M. Jeong, Z. M. Hassan, T. Islamoglu, H. Baumgart, A. J. McGaughey, E. Redel, O. K. Farha, P. E. Hopkins, J. A. Malen, C. E. Wilmer, *Nat. Commun.* 2020, 11, 4010.
- [34] X.-L. Shi, J. Zou, Z.-G. Chen, Chem. Rev. 2020, 120, 7399.
- [35] G. Tan, L.-D. Zhao, M. G. Kanatzidis, Chem. Rev. 2016, 116, 12123.
- [36] D. Beretta, N. Neophytou, J. M. Hodges, M. G. Kanatzidis, D. Narducci, M. Martin-Gonzalez, M. Beekman, B. Balke, G. Cerretti, W. Tremel, A. Zevalkink, A. I. Hofmann, C. Müller, B. Dörling, M. Campoy-Quiles, M. Caironi, *Mater. Sci. Eng.: R: Rep.* 2019, 138, 100501.
- [37] N. Jia, X. Y. Tan, J. Xu, Q. Yan, M. G. Kanatzidis, Acc. Mater. Res. 2022, 3, 237.
- [38] M. Islamov, H. Babaei, R. Anderson, K. B. Sezginel, J. R. Long, A. J. McGaughey, D. A. Gomez-Gualdron, C. E. Wilmer, npj Comput. Mater. 2023, 9, 11.
- [39] J. Kwon, H. Ma, A. Giri, P. E. Hopkins, N. B. Shustova, Z. Tian, ACS Nano 2023, 17, 15222.
- [40] D. Liu, J. Purewal, J. Yang, A. Sudik, S. Maurer, U. Mueller, J. Ni, D. Siegel, Int. J. Hydrogen Energy 2012, 37, 6109.
- [41] X. Wang, R. Guo, D. Xu, J. Chung, M. Kaviany, B. Huang, J. Phys. Chem. C 2015, 119, 26000.
- [42] M. Islamov, H. Babaei, C. E. Wilmer, ACS Appl. Mater. Interfaces 2020, 12, 56172.
- [43] X. Zhang, J. Jiang, J. Phys. Chem. C 2013, 117, 18441.
- [44] H. Babaei, A. J. McGaughey, C. E. Wilmer, Chem. Sci. 2017, 8, 583.
- [45] H. Babaei, C. E. Wilmer, Phys. Rev. Lett. 2016, 116, 025902.
- [46] L. Han, M. Budge, P. A. Greaney, Comput. Mater. Sci. 2014, 94, 292.
- [47] H. Babaei, A. J. McGaughey, C. E. Wilmer, ACS Appl. Mater. Interfaces 2018. 10. 2400.
- [48] M. E. DeCoster, H. Babaei, S. S. Jung, Z. M. Hassan, J. T. Gaskins, A. Giri, E. M. Tiernan, J. A. Tomko, H. Baumgart, P. M. Norris, A. J. H. McGaughey, C. E. Wilmer, E. Redel, G. Giri, P. E. Hopkins, J. Am. Chem. Soc. 2022, 144, 3603.
- [49] K. J. Erickson, F. Léonard, V. Stavila, M. E. Foster, C. D. Spataru, R. E. Jones, B. M. Foley, P. E. Hopkins, M. D. Allendorf, A. A. Talin, Adv. Mater. 2015, 27, 3453.
- [50] A. Lamaire, J. Wieme, A. E. Hoffman, V. Van Speybroeck, *Faraday Discuss.* 2021, 225, 301.
- [51] S. Zhang, J. Liu, L. Liu, RSC Adv. 2021, 11, 36928.



- [52] R. Cheng, W. Li, W. Wei, J. Huang, S. Li, ACS Appl. Mater. Interfaces 2021, 13, 14141.
- [53] P. Ying, J. Zhang, Z. Zhong, J. Phys. Chem. C 2021, 125, 12991.
- [54] P. Ying, J. Zhang, X. Zhang, Z. Zhong, J. Phys. Chem. C 2020, 124, 6274.
- [55] J. Huang, X. Xia, X. Hu, S. Li, K. Liu, Int. J. Heat Mass Transfer 2019, 138, 11.
- [56] K. B. Sezginel, P. A. Asinger, H. Babaei, C. E. Wilmer, Chem. Mater. 2018. 30, 2281.
- [57] M. Islamov, P. Boone, H. Babaei, A. J. McGaughey, C. E. Wilmer, Chem. Sci. 2023, 14, 6592.
- [58] A. M. Evans, A. Giri, V. K. Sangwan, S. Xun, M. Bartnof, C. G. Torres-Castanedo, H. B. Balch, M. S. Rahn, N. P. Bradshaw, E. Vitaku, D. W. Burke, H. Li, M. J. Bedzyk, F. Wang, J.-L. Brédas, J. A. Malen, A. J. H. McGaughey, M. C. Hersam, W. R. Dichtel, P. E. Hopkins, *Nat. Mater.* 2021, 20, 1142.
- [59] S. Thakur, A. Giri, J. Mater. Chem. A 2023, 11, 18660.
- [60] S. Thakur, A. Giri, Mater. Horiz. 2023, 10, 5484.
- [61] A. Giri, P. E. Hopkins, Nano Lett. 2021, 21, 6188.
- [62] M. A. Rahman, C. J. Dionne, A. Giri, Nano Lett. 2022, 22, 8534.
- [63] F. Tan, S. Han, D. Peng, H. Wang, J. Yang, P. Zhao, X. Ye, X. Dong, Y. Zheng, N. Zheng, L. Gong, C. Liang, N. Frese, A. Gölzhäuser, H. Qi, S. Chen, W. Liu, Z. Zheng, J. Am. Chem. Soc. 2021, 143, 3927.
- [64] H. Ma, Z. Aamer, Z. Tian, Mater. Today Phys. 2021, 21, 100536.
- [65] M. A. Rahman, S. Thakur, P. E. Hopkins, A. Giri, J. Phys. Chem. C 2023, 127, 11157.
- [66] S. Wieser, T. Kamencek, J. P. Dürholt, R. Schmid, N. Bedoya-Martínez, E. Zojer, Adv. Theory Simul. 2021, 4, 2000211.
- [67] D. Feng, Y. Feng, Y. Liu, W. Zhang, Y. Yan, X. Zhang, J. Phys. Chem. C 2020, 124, 8386.
- [68] Y. Liu, Y. Feng, Z. Huang, X. Zhang, J. Phys. Chem. C 2016, 120, 17060.
- [69] H. Ma, Y. Ma, Z. Tian, ACS Appl. Polym. Mater 2019, 1, 2566.
- [70] C. J. Dionne, M. A. Rahman, P. E. Hopkins, A. Giri, Nano Lett. 2022, 22, 3071.

- [71] R. Mercado, R.-S. Fu, A. V. Yakutovich, L. Talirz, M. Haranczyk, B. Smit, Chem. Mater. 2018, 30, 5069.
- [72] J. Blakemore, J. Appl. Phys. 1982, 53, R123.
- [73] B. J. Smith, A. C. Overholts, N. Hwang, W. R. Dichtel, *Chem. Commun.* 2016, 52, 3690.
- [74] A. Giri, P. E. Hopkins, Nat. Mater. 2020, 19, 482.
- [75] J. C. Duda, P. E. Hopkins, Y. Shen, M. C. Gupta, Phys. Rev. Lett. 2013, 110. 015902.
- [76] X. Wang, C. D. Liman, N. D. Treat, M. L. Chabinyc, D. G. Cahill, Phys. Rev. B 2013, 88, 075310.
- [77] X. Qian, J. Zhou, G. Chen, Nat. Mater. 2021, 20, 1188.
- [78] D. R. Clarke, S. R. Phillpot, Mater. Today 2005, 8, 22.
- [79] T. Takabatake, K. Suekuni, T. Nakayama, E. Kaneshita, Rev. Mod. Phys. 2014, 86, 669.
- [80] S. Plimpton, J. Comput. Phys. 1995, 117, 1.
- [81] P. Boone, H. Babaei, C. E. Wilmer, J. Chem. Theory Comput. 2019, 15, 5579.
- [82] D. Surblys, H. Matsubara, G. Kikugawa, T. Ohara, Phys. Rev. E 2019, 99. 051301.
- [83] D. Surblys, H. Matsubara, G. Kikugawa, T. Ohara, J. Appl. Phys. 2021, 130, 21.
- [84] A. K. Rappé, C. J. Casewit, K. Colwell, W. A. Goddard III, W. M. Skiff, J. Am. Chem. Soc. 1992, 114, 10024.
- [85] P. G. Boyd, S. M. Moosavi, M. Witman, B. Smit, J. Phys. Chem. Lett. 2017, 8, 357.
- [86] A. P. Thompson, S. J. Plimpton, W. Mattson, J. Chem. Phys. 2009, 131, 154107.
- [87] D. P. Sellan, E. S. Landry, J. Turney, A. J. McGaughey, C. H. Amon, Phys. Rev. B 2010, 81, 214305.
- [88] T. F. Willems, C. H. Rycroft, M. Kazi, J. C. Meza, M. Haranczyk, Migroporous Mesoporous Mater. 2012, 149, 134.
- [89] O. Talu, A. L. Myers, AIChE J. 2001, 47, 1160.
- [90] D. Ongari, P. G. Boyd, S. Barthel, M. Witman, M. Haranczyk, B. Smit, Langmuir 2017, 33, 14529.